

Compressed sensing based MIMO UWB-OFDM SAR imaging using image fusion

MD ANOWAR HOSSAIN*, IBRAHIM ELSHAFIEY

Department of Electrical Engineering, King Saud University, Riyadh, Saudi Arabia

Multiple-input multiple-output (MIMO) synthetic aperture radar (SAR) has received significant attention to radar communities recently. However, only few attempts on compressed sensing based MIMO SAR have been reported. This paper presents a novel scheme for wide-swath and high-resolution SAR based on MIMO ultra-wideband (UWB) orthogonal frequency division multiplexing (OFDM) system using compressed sensing (CS) technique. The swath is increased based on a new approach for orthogonal pulse-shaping and MIMO wide-swath stripmap SAR topology. The resolution is improved by using UWB-OFDM waveforms and the computational complexity is reduced by adopting the CS approach. CS based sparse imaging method is developed to deal with MIMO UWB-OFDM SAR using orthogonal matching pursuit (OMP) algorithm. Super-resolution property and image reconstruction ability are demonstrated using simulated data. Simulation results are provided to demonstrate the performance improvement of the proposed methods. Results show that the presented CS method outperforms the conventional matched filter (MF) based SAR imaging algorithm even though small amount of samples from SAR echo is used. Simulation results of conventional MF based SAR are also provided for fair comparisons. Performance is further enhanced using image fusion techniques to benefit from the potentials of multi-sensor imagery such as noise level reduction.

(Received May 6, 2014; accepted July 10, 2014)

Keywords: Compressed Sensing (CS); Synthetic Aperture Radar (SAR); Ultra-wideband (UWB); Multiple Input Multiple Output (MIMO); Orthogonal Frequency Division Multiplexing (OFDM); Image Fusion

1. Introduction

The idea behind SAR comes from the desire for high resolution images of the target area. SAR transmits pulse at spaced intervals called pulse repetition interval (PRI). The reflections at each PRI are stored and processed together to reconstruct an image of the terrain [1]. In general, high-resolution SAR images are obtained by transmitting ultra-wideband waveforms as radar pulse [2]. UWB waveforms (500 MHz bandwidth and above) can improve the range resolution of the SAR image. UWB technique provides dual advantages: good capacity of penetration and high resolution in range domain.

OFDM technique shows a great potential to be used in forming radar waveforms. An OFDM signal is comprised of several orthogonal sub-carriers, which are simultaneously transmitted over a single transmission path. Each subcarrier occupies a small portion of the entire signal bandwidth [3]. Feasibility study of OFDM based SAR has been investigated recently [4-9].

Although SAR imaging is an efficient remote sensing application, conventional single antenna SAR is not able to provide some required remote sensing performance, such as simultaneously high-resolution and wide-swath imaging. MIMO SAR provides a solution to resolve this drawback and provides following advantages as compared to traditional SAR: diversity in viewing angles on a particular target to improve identifiability, increased azimuth resolution or a decreased pulse repetition

frequency (PRF) which results in wider swath [10, 11]. Several research works have been done recently to overcome the trade-off between wide-swath and azimuth resolution in conventional SAR system. MIMO SAR systems are proposed by generalizing the theoretical modeling of MIMO communication systems and discussed recently in radar communities [12-14].

MIMO SAR can obtain simultaneous high-resolution and wide-swath imaging. However, a large amount of echo samples from multiple antennas must be collected and processed which leads to an excessive burden on the conventional MF based MIMO SAR imaging processor. CS is a new tool that intends to reconstruct the original signal by using just a few measurements beyond the Nyquist sampling constraints. It reduces the computational complexity and improves reconstruction results as compared to traditional MF based SAR imaging systems. Moreover, super-resolution can be achieved by employing the sparsity of the target based on CS theory.

CS has been widely used in many applications due to its compressed sampling and exact reconstruction ability. Some applications in radar field are as follows: Compressive radar imaging is addressed in [15]. Performance of CS for MIMO-OFDM radar is analyzed in [16]. CS based random frequency SAR imaging is introduced in [17]. An imaging algorithm for high-resolution and wide-swath space-borne SAR using CS on azimuth displacement phase center antenna (DPCA) is described in [18]. CS based image fusion technique is

developed in [19]. We can see that CS has been getting more attention in radar applications, such as to reduce the sampling burden and improve the resolution of radar system. Essentially, this article opens new prospects for MIMO SAR waveforms by focusing on the OFDM signal, and shows how this concept fits in a natural way with CS as a processing tool.

The increasing availability of spaceborne sensor motivates to use the image fusion algorithms. Several scenarios in image processing require higher spatial and spectral resolution in a single image. Image fusion is the process of combining relevant information from two or more images into a single image. The resulting image will be more informative than any of the input images [20].

The structure of the paper is as follows: MIMO UWB-OFDM pulse shaping is described in section 2. Detailed analysis of MIMO wide-swath SAR imaging topology and its functionality is discussed in section 3. CS based UWB-OFDM SAR imaging method is introduced in section 4. UWB-OFDM SAR imaging results based on conventional MF method and CS method and their comparison is presented in section 5. Section 6 presents the image fusion based optimization of MIMO UWB-OFDM SAR imaging technique. Final conclusion is given in section 7.

2. MIMO UWB-OFDM signal generation

A widely studied approach in MIMO architecture involves the transmission of orthogonal signals on the different antennas. This ensures the separation of reflected signals from the targets arriving at the receiver. In particular, we introduce a technique to design the optimal waveform that ensures orthogonality by applying the rules shown in Table 1. The key to our developed scheme is to use a model for the radar echo signals that explicitly includes the transmitted pulses. To achieve low cross-correlations between transmitted pulses with a common bandwidth for the same range resolution, OFDM frequency-domain sample vector for N sub-carriers is generated using the sequences as follows:

Table 1. OFDM frequency-domain vector generation.

	1	2	3	-	-	-	-	-	-	-	-	-	-	-	N
Ψ_{ω_1}	1	0	0	0	0	0	0	0	1	0	0	0	0	0	0
Ψ_{ω_2}	0	0	1	0	0	0	0	0	0	0	1	0	0	0	0
Ψ_{ω_3}	0	0	0	0	1	0	0	0	0	0	0	0	1	0	0
Ψ_{ω_4}	0	0	0	0	0	0	1	0	0	0	0	0	0	0	1

The sequences in Table 1 generate the orthogonal waveforms based on the orientation of 1's and 0's. It is observed that in each column, if we have a 1, the other elements are filled with 0's and the next column is filled with all 0's to prevent oversampling. The spectrum of an OFDM signal is shown in Fig. 1 where the width of the main-lobe depends on the pulse duration. In digital

implementation of OFDM signal, the pulse duration is related to the number of sub-carriers. As the number of sub-carrier increases, the duration of the pulse increases.

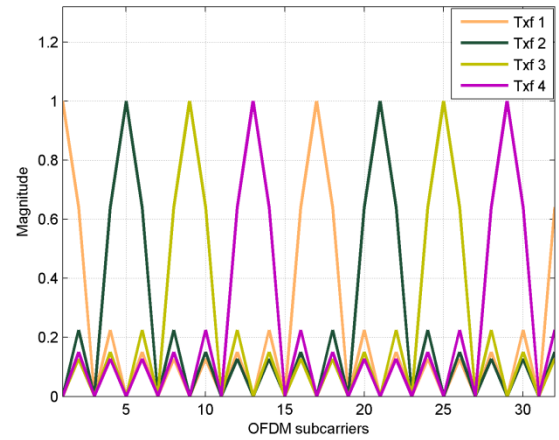


Fig. 1. OFDM signal spectrum.

For example, an OFDM signal can be generated by spreading the digital frequency domain vector shown in Table 1. The order of modulation (M) is chosen as 4 for QPSK. IFFT is then applied to obtain the discrete time domain OFDM signal and finally Hanning window is imposed to minimize the side-lobes. The time-domain OFDM signal is given as

$$\Psi_{txi}(t) = F^{-1}[\Psi_{\omega_i}] w(n) \quad i = 1, 2, \dots, 4 \quad (1)$$

where, Hanning window is given as

$w(n) = 0.5 \left\{ 1 - \cos \left(\frac{2\pi n}{N} \right) \right\}$, $0 \leq n \leq N - 1$ and N is the number of sub-carriers. The term Ψ_{ω_i} denotes the spreading sequences for i^{th} sub-pulses.

UWB-OFDM waveforms can be generated using the following parameters: number of OFDM sub-carriers, $N = 256$, sampling time, $\Delta t_s = 1$ ns results in baseband bandwidth, $B_0 = 1/2\Delta t_s = 500$ MHz, dividing by a factor of two to satisfy Nyquist criterion.

3. MIMO wide-swath SAR imaging topology

Let us consider a MIMO SAR system with transmit and receive array (possibly the same array) equipped with 2 co-located antennas. It is assumed that both transmit and receive arrays are close to each other in space but they illuminate different target area at different directions. Fig. 2 shows the MIMO wide-swath stripmap SAR imaging topology. The antenna beam A and B are illuminating the swath A and B respectively. At specific PRI, TxA transmits the pulse $\Psi_{txA}(t)$ via the antenna beam A, while TxB transmits the pulse $\Psi_{txB}(t)$ via the antenna beam B at the same time. Echoes from swath A and B exist at the both receivers. To separate echoes from swath A and B, an appropriate design of transmit antenna pattern as well as transmitted pulse is required. It can also reduce the interference from the undesired swath.

We consider four orthogonal sub-pulses based on the sample vectors shown in Table 1. Two different signals $\Psi_{txA}(t)$ and $\Psi_{txB}(t)$ are transmitted simultaneously from antenna *A* and *B* respectively at each PRI where each signal is the combination of two sub-pulses and are given as

$$\Psi_{txA}(t) = \Psi_{tx1}(t) + \Psi_{tx2}(t) \quad (2)$$

$$\Psi_{txB}(t) = \Psi_{tx3}(t) + \Psi_{tx4}(t) \quad (3)$$

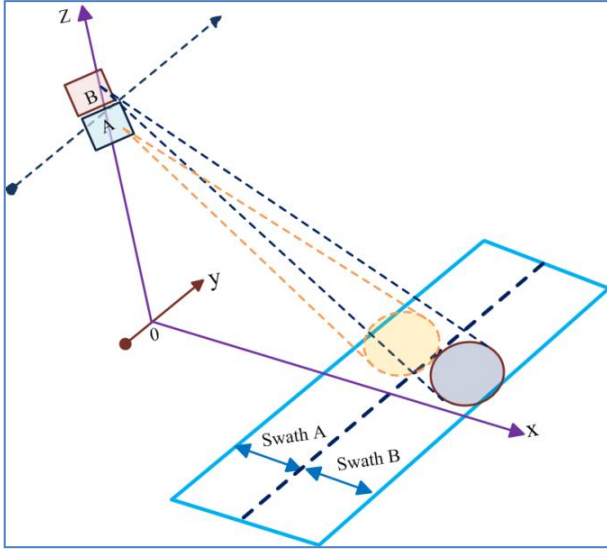


Fig. 2. MIMO stripmap wide-swath SAR topology.

The received signal for radar at antenna *A* is given by

$$\Psi_{rxA}(t, u) = \left[\sum_{n=1}^N \sigma_n \Psi_{txA}(t - t_{dnA}) \right] + \beta \left[\sum_{n=1}^N \sigma_n \Psi_{txB}(t - t_{dnB}) \right] + \eta_A(t) \quad (4)$$

Similarly, the received signal at antenna *B* is given as

$$\Psi_{rxB}(t, u) = \left[\sum_{n=1}^N \sigma_n \Psi_{txB}(t - t_{dnB}) \right] + \beta \left[\sum_{n=1}^N \sigma_n \Psi_{txA}(t - t_{dnA}) \right] + \eta_B(t) \quad (5)$$

where, α and β are the scale factor and is chosen as $\frac{1}{\sqrt{2}}$ and $\frac{1}{\sqrt{10}}$ respectively. The scale factor α is considered to distribute the total power to two sub-pulses and β is used to compensate for the out-of-beam signal.

The term $t_{dnA} = \frac{2}{c} \sqrt{(X_{cA} + x_n)^2 + (y_n - u)^2}$ is the time-delay associated with the target position (x_n, y_n) in swath *A* and $t_{dnB} = \frac{2}{c} \sqrt{(X_{cB} + x_n)^2 + (y_n - u)^2}$ is the time-delay associated with swath *B*. X_{cA} and X_{cB} denote the range distance to the center of the swath *A* and *B* respectively, where, $n = 1, 2, 3, \dots, N$ are the number of targets within the antenna beam at any given synthetic aperture position (u) in azimuth direction while σ_n denotes the reflectivity of

the n^{th} target. The terms $\eta_A(t)$ and $\eta_B(t)$ denote the additive white Gaussian noise.

The received echoes are separated apart by matched filtering. As the transmitted signal matrix is known to both transmitter and receiver and the transmitted waveforms are designed to be orthogonal, they should satisfy the conditions

$$\int_0^{T_p} \Psi_{rxm}(t) \Psi_{txn}^*(t) dt = \begin{cases} \delta(t), & m = n \\ 0, & m \neq n \end{cases} \quad (6)$$

where, T_p is the sub-pulse duration and $(.)^*$ denotes a conjugate operator. At receiving antenna *A*, two received orthogonal sub-pulses can be extracted by two matched filters and is given by

$$\Psi_{MFn}(t) = F^{-1} [F\{\Psi_{rxA}(t)\} \cdot F\{\Psi_{txn}^*(t)\}] \quad (7)$$

Similarly, at receiving antenna *B*, two sub-pulses can be separated as

$$\Psi_{MFn}(t) = F^{-1} [F\{\Psi_{rxB}(t)\} \cdot F\{\Psi_{txn}^*(t)\}] \quad (8)$$

where, $n = 1, 2$ for equation (7) and $n = 3, 4$ for equation (8) while F^{-1} and F denote the inverse Fourier transform and Fourier transform operations respectively. Therefore, echoes from two swaths could be considered as well separated after the matched filtering.

Finally, we have a total of four received signals from two receiving antennas. Compared to the conventional phased array SAR where the same waveform is used at all the transmitting antennas and a total of 2 coefficients obtained for the matched filtering, the proposed MIMO OFDM SAR gives more coefficients and therefore provides more degrees of freedom. Each matched filter output is then processed separately using SAR imaging algorithms such as Range-Doppler algorithm (RDA) or OMP based sparse target imaging method. Finally, image fusion technique is applied to optimize the SAR image.

4. Compressed sensing for UWB-OFDM SAR

In some special applications, (such as ocean ships monitoring, aircraft and spacecraft detecting) the number of dominant scatterers is much smaller than the number of overall samples. In such a case, SAR echo can be regarded as sparse signal. Thereby, a sparse reconstruction based on CS can be used in these applications.

High-resolution imaging with SAR can be achieved by using UWB-OFDM waveforms. However, due to higher sampling speed of UWB scale, it leads to extremely high data rate on SAR imaging processor. Sparse sampling method based on compressed sensing (CS) theory is used, by which only a small amount of radar echoes are used for SAR imaging. The raw echo signal of each channel can be reconstructed for SAR imaging with high probability by using OMP algorithm. This indicates the sample size of SAR echoes can be considerably reduced by CS method.

OMP is an iterative greedy algorithm that selects the column which is most correlated with the current residuals at each step [21-23]. For a given measurement matrix $\Psi \in \mathbb{R}^{m \times n}$ ($n > m$), the CS recovery algorithm generates an estimate of K -sparse vector $x \in \mathbb{R}^n$ from a set of linear measurements given as

$$y = \Psi x + \varepsilon \quad (9)$$

where, y is the measurement vector, Ψ denotes the measurement matrix, x is the original signal to be recovered and ε denotes the amount of noise. Due to the prior information of signal sparsity, x can be perfectly recovered using efficient recovery algorithm. Among many recovery algorithms in the literature, a greedy method receives significant attention for practical benefits. The OMP algorithm has received significant interest because of its simplicity and efficient recovery performance. It has also been shown that the Orthogonal Matching Pursuit (OMP) is reliable for reconstructing both sparse and near-sparse signals [24]. OMP estimates the sparse signal as

$$\hat{x} = \arg \min_x \|y - \Psi x\|_2 \quad (10)$$

A widely used framework for OMP based sparse signal recovery is the *Mutual Incoherence Property* (MIP) and is defined by

$$\mu = \max_{i \neq j} |\langle \Psi_i, \Psi_j \rangle| \quad (11)$$

where, Ψ_i and Ψ_j denote the i^{th} and j^{th} column of Ψ respectively.

The advantage of using OFDM signal in Orthogonal Matching Pursuit (OMP) based SAR imaging is that it ensures the *Mutual Incoherence Property* (MIP) to be small enough because the SAR system transmits a unique pulse at each PRI by using random sub-carrier composition. Moreover, it ensures lower cross-correlation (CCF) properties among the pulses. The procedure for CS based SAR image reconstruction used in this article is as follows:

- i) Generating SAR raw echoes considering point targets at each cell of the target area.
- ii) Randomly select a small amount of raw echoes to create measurement matrix (Ψ).
- iii) Creating sparse signal (x) and computing observation vector (y).
- iv) Signal recovery using OMP (\hat{x}).
- v) 2D SAR imaging of sparse targets.

5. SAR imaging using CS and RDA

The scenario involves the UWB-OFDM SAR imaging of two distinct target-maps in swath A and swath B. The aim is to verify the imaging capability of the orthogonal waveforms as SAR transmitted pulse. Let us consider 9 point targets reside in swath A while a battle tank with 4 point targets in swath B as shown in Fig. 3.

Stripmap SAR imaging topology is used for raw data generation based on the proposed UWB-OFDM waveform as SAR transmitted pulse while Range-Doppler algorithm (RDA) [25] and Orthogonal Matching Pursuit (OMP) based CS method is used for SAR image reconstruction. The imaging results of 9 point targets using both MF based RDA and the CS method without noise and SNR = 20 dB is shown in Fig. 4 and Fig. 5 respectively. It is observed that the significant sidelobe interference in RDA based imaging and the situation is worse when the distances among the targets are close to each other (5 point targets at the center) as shown in Fig. 4. On the other hand, the actual targets position and amplitudes are perfectly reconstructed using CS method as shown in Fig. 5. The sidelobe interference is far less than that in RDA method.

Fig. 6 shows the imaging of extended targets as shown in Fig. 3(b). The imaging result shows that the position and scattering coefficients are clearly reconstructed with CS as compared to RDA. The performance of the CS method in the noisy environments depends on the number of measurements. Fig. 7 shows the effects of amount of echo samples used in CS method with SNR = 20 dB. We observe that the scattering centers are reconstructed with higher amplitudes when larger number of echo samples (50%) is used.



Fig. 3. Simulated scene. (a) 9 point targets in swath A. (b) 2D battle tank and 4 point targets in swath B.

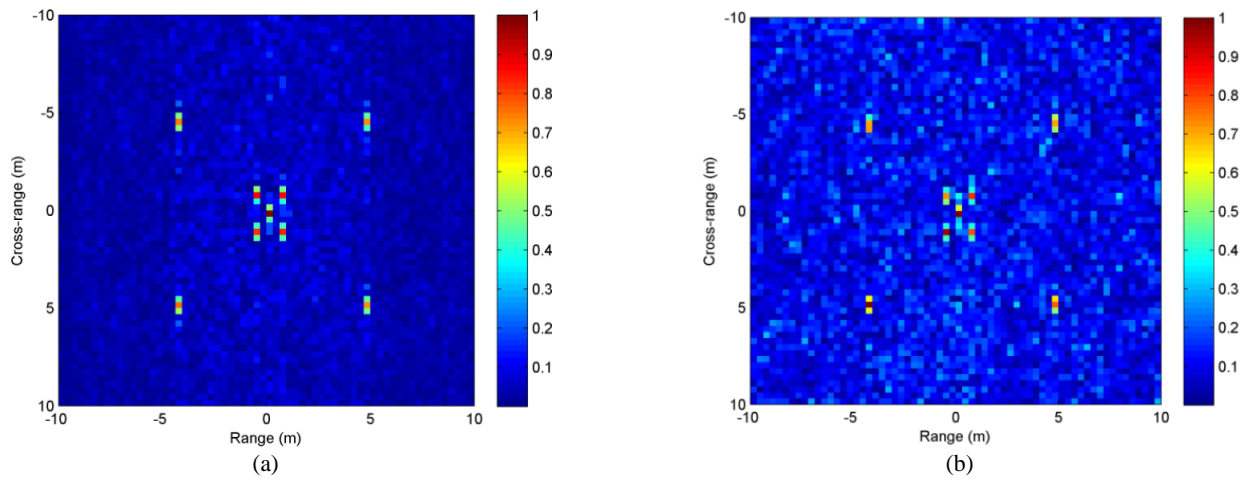


Fig. 4. MF based imaging results using all echo samples (a) Noise free. (b) SNR = 20 dB.

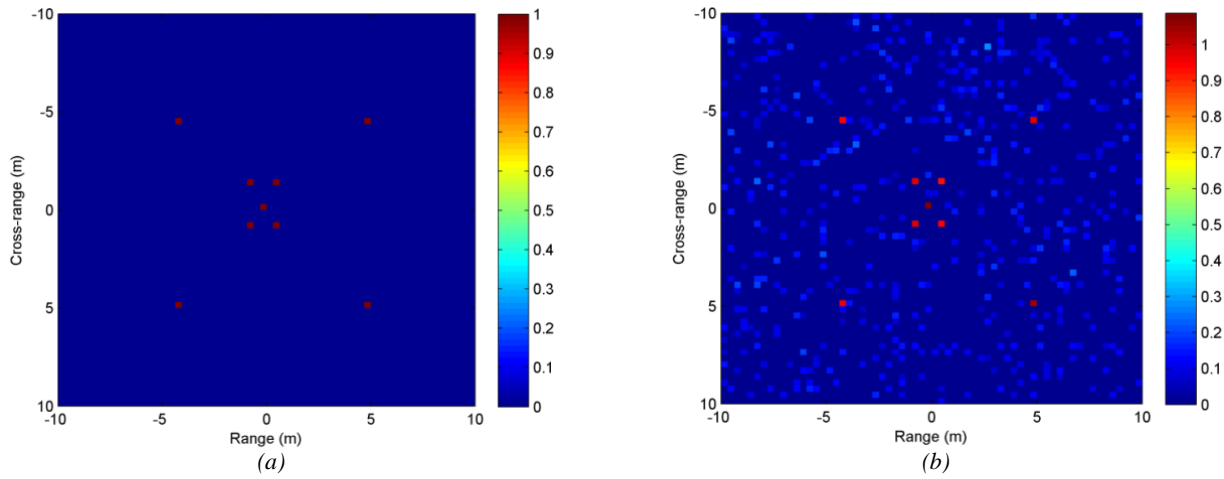


Fig. 5. CS based results using only 10% echo samples. (a) Noise free (b) SNR = 20 dB.

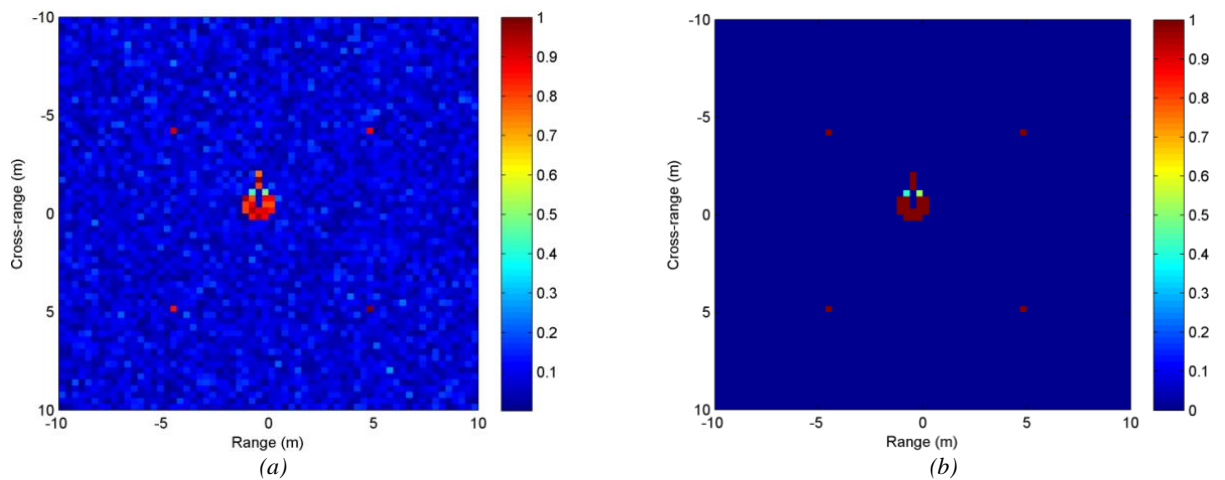


Fig. 6. Imaging results of extended targets without noise. (a) MF based reconstruction using all echo samples (b) CS based reconstruction using 25% of echo samples.

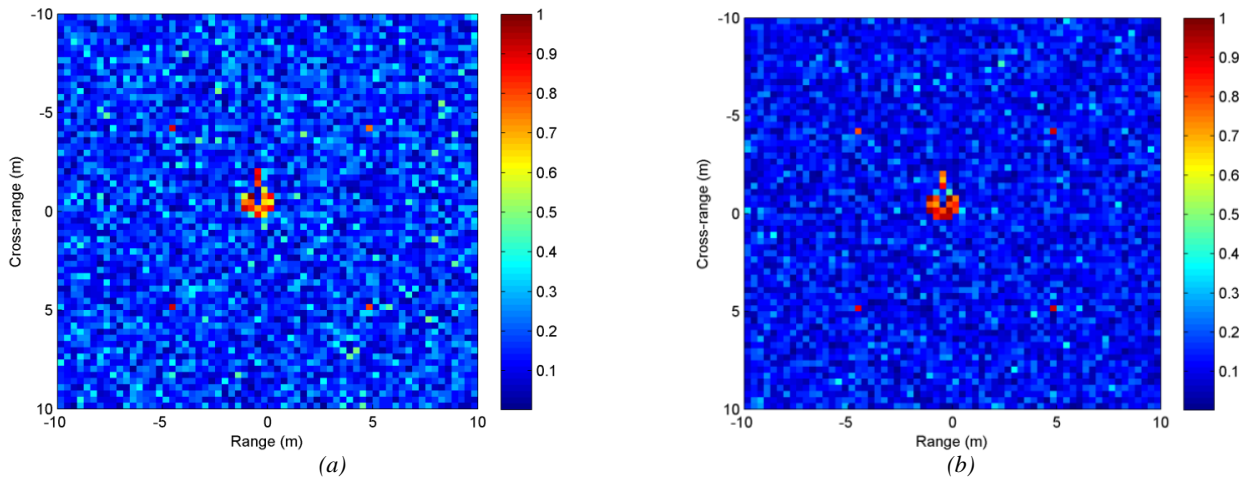


Fig. 7. CS based imaging of extended targets with SNR = 20 dB. (a) Using 25% echo samples (b) Using 50% of echo samples.

6. Image fusion based MIMO UWB-OFDM SAR Imaging

Observing a target area of interest from two antennas with different trajectories allows us to determine the position of the scattering points. SAR interferometry fails when the scenes imaged by the two antennas are not really the same scene, due to a too large distance between the trajectories of the two SAR antennas. Thus, two SAR images may not be sufficiently correlated. So, we consider the SAR image fusion using the raw data obtained by two antennas from the same target area using two sub-pulses simultaneously. The usefulness of the image fusion is verified by estimating the noise level in terms of entropy for the non-fused and fused SAR images.

In all wavelet based image fusion schemes the DWT of the two registered input images $I_1(x, y)$ and $I_2(x, y)$ are computed and these transforms are combined using some kind of fusion rule. Then the inverse discrete wavelet

transform (IDWT) is computed and the fused image $I(x, y)$ is reconstructed as

$$I(x, y) = W^{-1}[\phi\{W(I_1(x, y)), W(I_2(x, y))\}] \quad (12)$$

where, W and W^{-1} denotes the DWT and IDWT respectively. The term ϕ denotes the fusion rules such as wavelet function, level, approximation, and detail coefficients.

Fig. 8 shows the block diagram of the image fusion based MIMO UWB-OFDM SAR imaging system. As described in section 3, at each PRI, two received signals are extracted from each receiving antenna. So, we have four sets of raw echoes. The raw data obtained from multiple antennas can be processed in parallel. Finally, we have two SAR images for each swath which can be fused together.

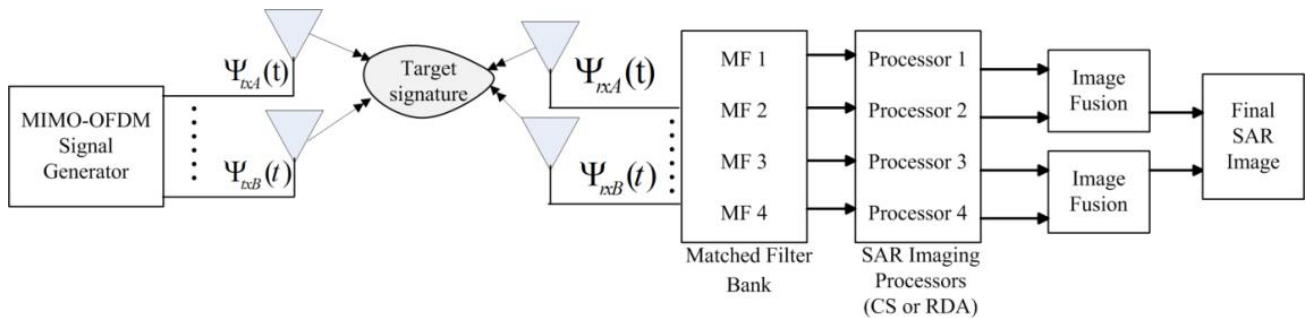


Fig. 8. Block diagram of image fusion based MIMO UWB-OFDM SAR

Fig. 9 shows the reconstructed images of swath A and B using the extracted raw echoes of different matched filters. Fig. 10(a) shows the fused image obtained by using the resolved images of matched filter 1 and 2 while Fig. 10(b) shows the fused image using the images obtained by the output of matched filter 3 and 4. Since wavelet coefficients with large absolute values contain the information about the salient features of the images such

as edges and lines, a good fusion rule is to choose the 'maximum' for 'approximation' values, while 'minimum' is chosen for the 'details' to suppress the noise. Final reconstructed wide-swath SAR image shown in Fig. 11 with all resolved point targets of swath A and B is the horizontal concatenation of fused images of Fig.10.

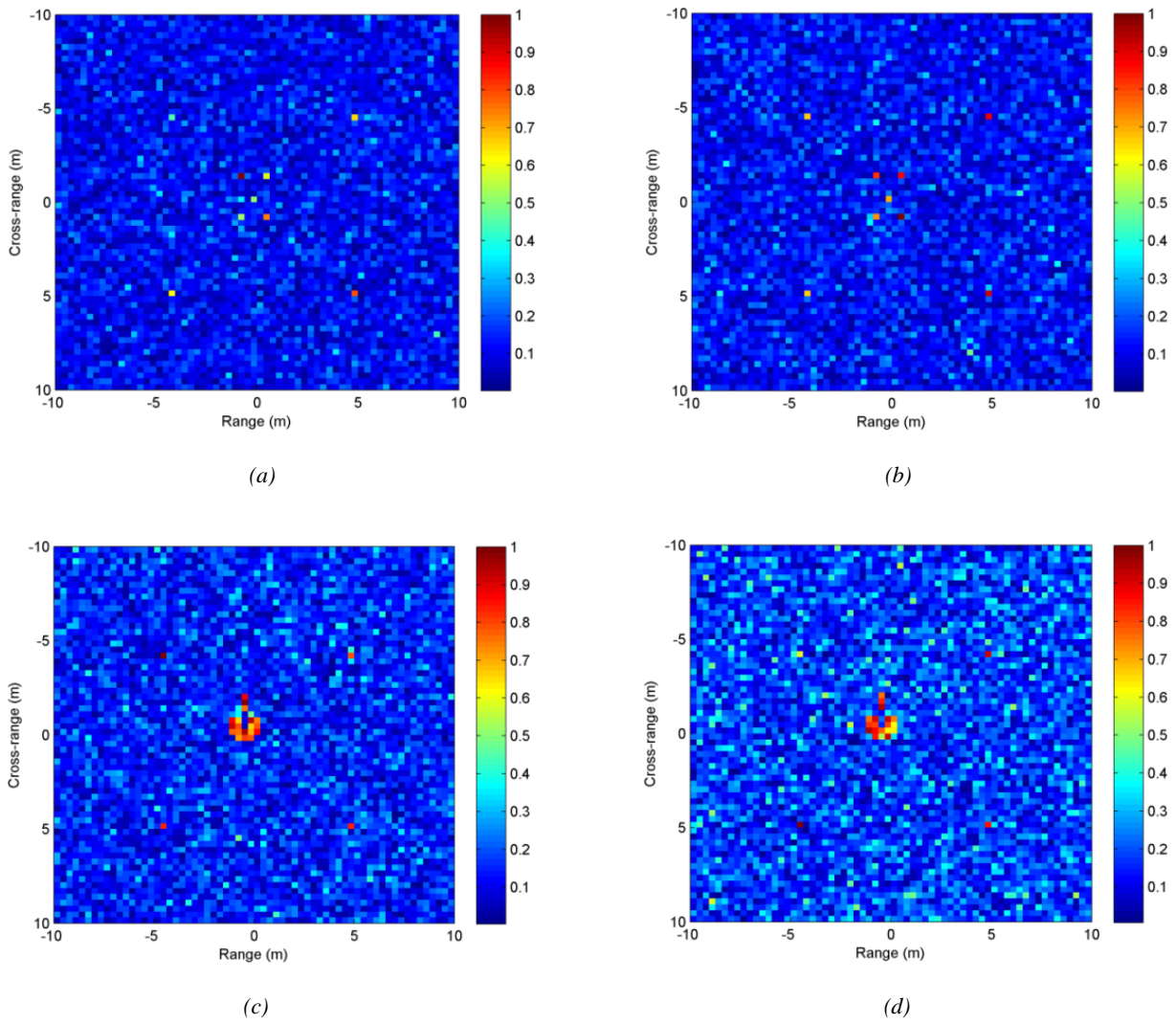


Fig. 9. Imaging results (SNR = 10 dB) using raw echoes from different MF output. (a) MF1, Swath A (b) MF2, Swath A (c) MF3, Swath B. (d) MF4, Swath B.

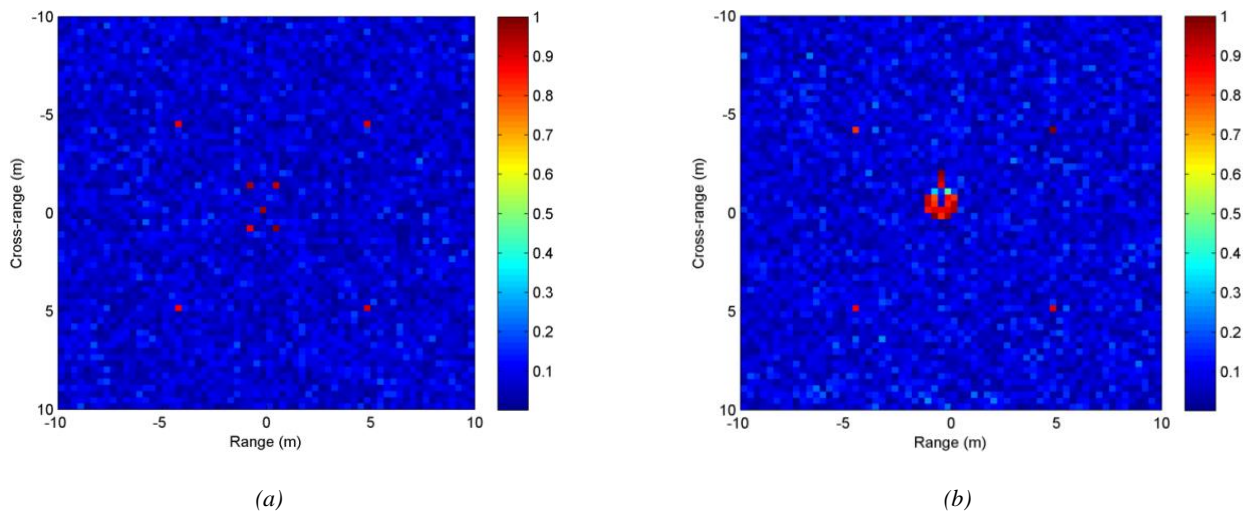


Fig. 10. Fused images (a) Using MF1 and MF2 output (Swath A). (b) Using MF3 and MF4 output (Swath B).

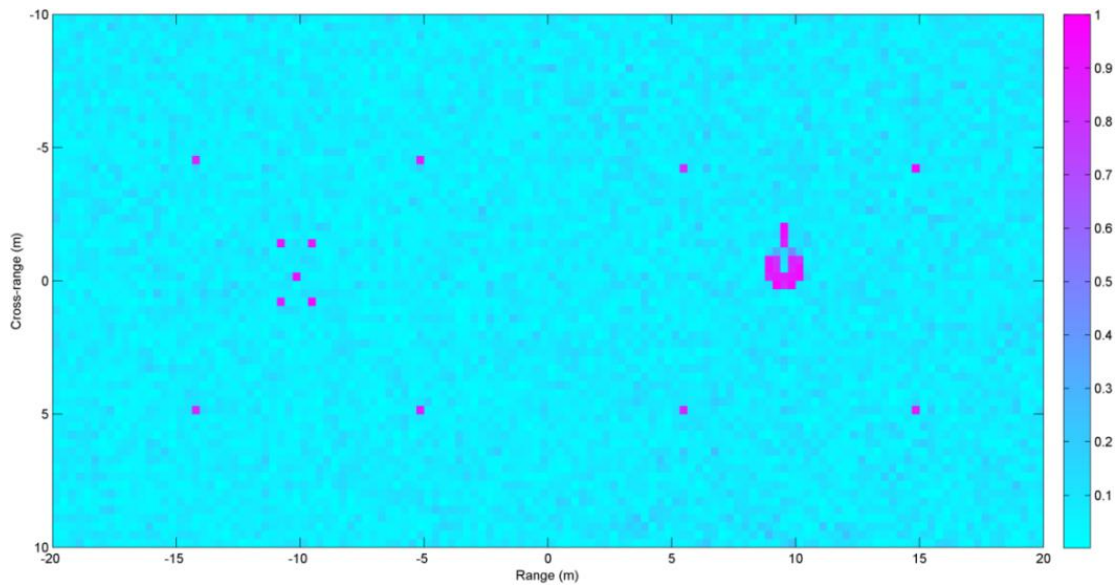


Fig. 11. Final SAR image.

To verify the minimization of noise level after the image fusion, the input images and fused image are evaluated in terms of entropy. Entropy is a good measure for information content (uncertainty) of the image. Information content in SAR images after wavelet transform based image fusion is identified with entropy

value that serves as a measure of the roughness present in the image space. Entropy is used as a measurement of noise level in non-fused and fused images. Table 2 provides the entropy of the input images and fused images for different types of wavelets. It is observed that the Haar wavelet gives the more reduction in noise level.

Table 2. Entropy of SAR images before and after fusion.

Wavelet	Parameters	Entropy of image 1	Entropy of image 2	Entropy of fused image (Swath A)	Entropy of fused image (Swath B)
Haar	Level : 5 Approx.: Max Details: Min	(Swath A)	(Swath A)	4.9572	4.8627
Daubechies1		5.6353	5.6072	4.9574	4.8630
Symlets2		(Swath B)	(Swath B)	4.9594	4.8696
Coiflets2		5.5606	5.5362	4.9605	4.8723

7. Conclusion

A compressed sensing based MIMO UWB-OFDM SAR system wide-swath imaging capability has been investigated. Pulse shaping is a crucial part of OFDM applications. As orthogonal transmission waveforms are required for the proposed MIMO OFDM SAR system, a new approach to generate OFDM waveforms is explored and investigated. CS approach has been adopted to reduce the processing complexity of raw SAR data and super-resolution property is demonstrated. It is shown that the proposed MIMO UWB-OFDM SAR indeed provides a potential solution to high-resolution remote sensing as well as wide-swath imaging. The effectiveness of the proposed method was demonstrated by SAR image fusion. Image fusion techniques provide a powerful tool to reduce the noise level and improve the SAR images.

Acknowledgement

This work is funded by the National Plan for Science and Technology, Kingdom of Saudi Arabia, under project number: 10-ELE996-02.

References

- [1] M. Soumekh, Synthetic aperture radar signal processing, Wiley New York, 1999.
- [2] S. R. Wood, R. Aiello, Essentials of UWB, Cambridge University Press New York, 2008.
- [3] L. Hanzo, M. Münster, B. Choi, T. Keller, OFDM and MC-CDMA, Wiley, March, 2004.
- [4] M. A. Hossain, I. Elshafiey, M. A. Alkanhal, High resolution UWB SAR based on OFDM architecture, in Synthetic Aperture Radar (AP SAR), 2011 3rd International Asia-Pacific Conference, p. 1, 2011.
- [5] M. A. Hossain, I. Elshafiey, M. A. Alkanhal, A. Mabrouk, Adaptive UWB-OFDM synthetic aperture

- radar, Electronics, Communications and Photonics Conference (SIEPCPC), 2011 Saudi International, p. 1, 2011.
- [6] M. A. Hossain, I. Elshafiey, M. A. Alkanhal, A. Mabrouk, Anti-jamming capabilities of UWB-OFDM SAR, Radar Conference (EuRAD), 2011 European, p. 313, 2011.
- [7] M. A. Hossain, I. Elshafiey, M. A. Alkanhal, A. Mabrouk, Real-time implementation of UWB-OFDM synthetic aperture radar imaging, Signal and Image Processing Applications (ICSIPA), 2011 IEEE International Conference on, p. 450, 2011.
- [8] W.-Q. Wang, OFDM waveform diversity design for MIMO SAR imaging, Geoscience and Remote Sensing Symposium (IGARSS), 2012 IEEE International, p. 2090, 2012.
- [9] W.-Q. Wang, Geoscience and Remote Sensing Letters, IEEE, **10**, 101 (2013).
- [10] W.-Q. Wang, Geoscience and Remote Sensing, IEEE Transactions, **49**, 3094 (2011).
- [11] W.-Q. Wang, Large-area remote sensing in high-altitude high-speed platform using MIMO SAR, 2013.
- [12] J. H. Ender and J. Klare, System architectures and algorithms for radar imaging by MIMO-SAR, Radar Conference, 2009 IEEE, p. 1, 2009.
- [13] S. Lim, C. Hwang, S. Kim, N. Myung, Journal of Electromagnetic Waves and Applications, **25**, 1168 (2011).
- [14] W. Xu, P. Huang, Y.-K. Deng, Progress In Electromagnetics Research, **121**, 2011.
- [15] R. Baraniuk, P. Steeghs, Compressive radar imaging, Radar Conference, 2007 IEEE, p. 128, 2007.
- [16] C. R. Berger, S. Zhou, P. Willett, B. Demissie, J. Heckenbach, Compressed sensing for OFDM/MIMO radar, Signals, Systems and Computers, 2008 42nd Asilomar Conference, p. 213, 2008.
- [17] J. Yang, J. Thompson, X. Huang, T. Jin, Z. Zhou, Geoscience and Remote Sensing, IEEE Transactions, **51**, 983 (2013).
- [18] J. Chen, J. Gao, Y. Zhu, W. Yang, P. Wang, Progress In Electromagnetics Research, **125**, 2012.
- [19] T. Wan, N. Canagarajah, A. Achim, Compressive image fusion, Image Processing, 2008. ICIP 2008. 15th IEEE International Conference, p. 1308, 2008.
- [20] I. Elshafiey, A. Algarni, M. A. Alkanhal, Image fusion based enhancement of nondestructive evaluation systems, Ch11 in Image Fusion, 2011.
- [21] T. T. Cai, L. Wang, Information Theory, IEEE Transactions, **57**, 4680, 2011.
- [22] J. A. Tropp, Information Theory, IEEE Transactions on, **50**, 2231 (2004).
- [23] J. A. Tropp, A. C. Gilbert, Information Theory, IEEE Transactions on, **53**, 4655 (2007).
- [24] N. Aravind, K. Abhinandan, V. Acharya, D. Sumam, Comparison of OMP and SOMP in the reconstruction of compressively sensed hyperspectral images, Communications and Signal Processing (ICCSP), 2011 International Conference, p. 188, 2011.
- [25] I. G. Cumming, F. H. Wong, Digital signal processing of synthetic aperture radar data: algorithms and implementation, Artech House, 2004.

*Corresponding author: ahossain@ksu.edu.sa